Original Article

DOI: 10.5582/bst.2019.01230

Suppression of tumor growth and metastasis by ethanol extract of *Angelica dahurica Radix* in murine melanoma B16F10 cells

Hyun Hwangbo[1,2], Eun Ok Choi[1,2], Min Yeong Kim[1,2], Da Hye Kwon[1,2], Seon Yeong Ji[1,2], Hyesook Lee[1,2], Sang Hoon Hong[3], Gi-Young Kim[4], Hye Jin Hwang[5], Su Hyun Hong[1,2], Yung Hyun Choi[1,2,*]

[1] Anti-Aging Research Center, Dong-eui University, Busan, Korea;
[2] Department of Biochemistry, Dong-eui University College of Korean Medicine, Busan, Korea;
[3] Department of Internal Medicine, Dong-eui University College of Korean Medicine, Busan, Korea;
[4] Department of Marine Life Sciences, Jeju National University, Jeju, Korea;
[5] Department of Food and Nutrition, Dong-eui University, Busan, Korea.

SUMMARY The roots of *Angelica dahurica* have long been used as a traditional medicine in Korea to treat various diseases such as toothache and cold. In this study, we investigated the effect of ethanol extract from the roots of this plant on metastatic melanoma, a highly aggressive skin cancer, in B16F10 melanoma cells and B16F10 cell inoculated-C57BL/6 mice. Our results showed that the ethanol extracts of *Angelicae dahuricae Radix* (EEAD) suppressed cell growth and induced apoptotic cell death in B16F10 cells. EEAD also activated the mitochondria-mediated intrinsic apoptosis pathway, with decreased mitochondrial membrane potential, and increased production of intracellular reactive oxygen species and ration of Bax/Bcl-2 expression. Furthermore, EEAD reduced the migration, invasion, and colony formation of B16F10 cells through the reduced expression and activity of matrix metalloproteinase (MMP)-2 and -9. In addition, *in vivo* results demonstrated that oral administration of EEAD inhibited lactate dehydrogenase activity, hepatotoxicity, and nephrotoxicity without weight loss in B16F10 cell inoculated-mice. Importantly, EEAD was able to markedly suppress lung hypertrophy, the incidence of B16F10 cells lung metastasis, and the expression of tumor necrosis factor-alpha in lung tissue. Taken together, our findings suggest that EEAD may be useful for managing metastasis and growth of malignant cancers, including melanoma.

Keywords Angelica dahurica; B16F10 cells; apoptosis; invasion; lung metastasis

1. Introduction

Over the past several decades, the incidence and mortality rates of melanomas have increased rapidly, and the number of cases has increased more rapidly than other types of solid tumors. In particular, metastatic melanoma is the most aggressive tumor due to its unique ability to metastasize prematurely and resistance to conventional therapies (*1,2*). However, clinical management of patients with metastatic melanoma is limited to treatment, due to the absence of effective target chemotherapy and control protocols (*3,4*). Although various therapies have been developed for the treatment of patients with melanoma, chemotherapy is still the primary approach for blocking cancer metastasis. However, some limitations, such as adverse side effects, drug resistance, and limited efficacy, remain to be solved (*5,6*). Therefore, it is urgent to develop new therapeutic strategies that minimize these limitations and have high therapeutic efficacy. In this regard, interest in natural resources that have traditionally been used in the prevention and treatment of various diseases is increasing (*7*). In addition, some herbal extracts have been shown to induce apoptosis and inhibit the metastasis of cancer cells, which are important strategies for the control of proliferation in cancer cells, without showing toxicity to normal cells (*8,9*).

Angelica dahurica Radix, the roots of *Angelica dahurica* Bentham et Hooker, which belongs to the genus Angelica (family Apiaceae), is widely used as a traditional medicine to treat several symptoms including headaches, asthma, hypertension, colds, and toothaches in East Asian countries including Korea, Japan and China (*10-12*). Up to now, various therapeutic activities

of *Angelica dahurica Radix* including anti-microbial, anti-oxidant, anti-inflammatory, and anti-mutagenic effects have been reported (*13-18*). Although recent studies have showed that the extracts and/or compounds isolated *Angelica dahurica Radix* has an anti-tumor effect on human cancer cells (*17,19-22*), the underlying mechanism is not yet well known. Therefore, in this study, as part of a screening program for the discovery of traditional medicine resources with anti-metastatic activity, we investigated the effect of ethanol extract from the *Angelica dahurica Radix* on the metastatic potential of murine melanoma B16F10 cells and attempted to identify the mechanism of action.

2. Materials and Methods

2.1. Preparation of 70% ethanol extract of *Angelica dahurica Radix*

The dried roots of *A. dahurica* (*Angelica dahurica Radix*) were obtained from Dong-eui Korean Medical Center (Busan, Republic of Korea). The roots (100 g) were ground into fine powder, and refluxed with 1 L of 70% ethanol solution by sonication for 24 h. After filtering through a glass filter funnel to remove insoluble matters, the extracts were concentrated with a rotary vacuum evaporator (Buchi Labortechnik, Flawil, Switzerland) and followed by lyophilization. The ethanol extracts of *Angelicae dahuricae Radix* (abbreviated as EEAD hereafter) were then stored at -80°C prior to use. EEAD were dissolved in dimethylsulfoxide (DMSO, Sigma-Aldrich Chemical Co., St. Louis, MO, USA) to a final concentration of 100 mg/mL. The stock solution was diluted with a cell culture medium to the desired concentration before use.

2.2. Cell culture

B16F10 cells that originate in the syngeneic C57BL/6 (H-2b) mouse stain, were obtained from the American Type Culture Collection (Manassas, MD, USA). The cells were maintained in Dulbecco's modified Eagle's medium (DMEM) supplemented with 10% fetal bovine serum (FBS), 100 U/mL penicillin, and 100 μg/mL streptomycin (WelGENE Inc., Daegu, Republic of Korea).

2.3. Cell viability assay

Cell viability was assessed by 3-(4,5-dimethyl-2-thiazolyl)-2,5-diphenyltetra-zolium bromide (MTT) assay, as described previously (*19*). Briefly, B16F10 cells were seeded onto 96-well plates at a density of 1 × 10^4 cells/well, and incubated for overnight. The cells were exposed to a series of concentrations of EEAD for 24 h, and the cells were then incubated with 50 μg/mL MTT solution (Invitrogen, Waltham, MA, USA) at 37°C for 2 h. Subsequently, the medium was removed, and DMSO was added to each well to dissolve the formed blue formazan crystals, followed by measurement at 570 nm in a microplate reader (Molecular Device Co., Sunnyvale, CA, USA). The morphological changes of cells were directly observed and photographed under a phase-contrast microscope (Carl Zeiss, Oberkochen, Germany).

2.4. Nuclear staining assay

The alteration of nuclear morphology in EEAD-treated cells was assessed by 4′,6-diamidino-2-phenylindole (DAPI) staining. In brief, cells were treated with different concentrations of EEAD for 24 h, and then fixed with 4 % paraformaldehyde (Sigma-Aldrich Chemical Co.) at room temperature for 10 min. The cells were washed with phosphate buffered saline (PBS), and stained with 1 μg/m DAPI solution (Sigma-Aldrich Chemical Co.) for 10 min, under light-shielded conditions. The cells were rinsed with PBS, visualized and photographed using a fluorescence microscope (Carl Zeiss).

2.5. Determination of apoptotic cell death by flow cytometric analysis

The magnitude of apoptosis was measured by flow cytometry using the annexin V-fluorescein isothiocyanate (FITC) Apoptosis detection kit (BD Biosciences, San Diego, CA, USA). After treatment with EEAD for 24 h, the cells were suspended in the supplied binding buffer, and then stained with FITC-conjugated annexin V and propidium iodide (PI) for 20 min in the dark at room temperature, by following the manufacturer's protocol. The fluorescent intensities of the cells were detected by flow cytometry (BD Biosciences), and the annexin V^+/PI^- and annexin V^+/PI^+ cell populations were considered indicators of apoptotic cells.

2.6. Measurement of mitochondrial membrane potential (MMP, $\Delta\Psi m$)

To measure MMP ($\Delta\Psi m$), 5,5',6,6'-tetrachloro-1,1',3,3'-tetraethyl-imidacarbocyanine iodide (JC-1) staining was performed. After treatment with EEAD for 24 h, cells were exposed to 10 μM JC-1 (Sigma-Aldrich Chemical Co.) for 30 min at 37°C. The cells were washed with PBS to remove unbound dye, and the cells were collected for each sample. The amounts of MMP ($\Delta\Psi m$) were detected at 488/575 nm using a flow cytometer, according to the manufacturer's instruction.

2.7. Measurement of intracellular reactive oxygen species (ROS) production

The production of ROS was measured using 5,6-carboxy-2',7'-dichlorodihydrofluorescein diacetate

(DCF-DA), as described previously (*23*). After treatment with EEAD for 30 min, the cells were washed with PBS and incubated with 10 μM DCF-DA (Invitrogen) in the dark at 37°C for 20 min. Subsequently, the cells were analyzed for DCF fluorescence by flow cytometry at 480 nm/520 nm.

2.8. Reverse transcription-polymerase chain reaction (RT-PCR)

Total RNA was isolated using TRIzol reagent (Invitrogen) by the manufacturer's recommended protocol. After quantifying the RNA concentration, genes of interest were amplified from cDNA that was reverse-transcribed from 1 μg of total RNA using AccuPower® PCR PreMix (Bioneer, Daejeon, Korea), as described previously (*24*). The PCR was carried out using the Mastercycler (Eppendorf, Hamburg, Germany) under the following conditions: initial denaturation for 3 min at 94°C; 30 cycles of 30 sec at 94°C, 30 sec at 61°C, and 1 min at 72°C; and final extension for 5 min at 72°C. Subsequently, PCR products were separated on 1.0% agarose gel containing ethidium bromide (EtBr; Sigma-Aldrich Chemical Co.) and visualized using ultraviolet light. The glyceraldehyde 3-phosphate dehydrogenase (GAPDH) housekeeping gene transcript was used as a control.

2.9. Protein extraction and Western blot analysis

The whole cellular proteins were prepared using the Bradford protein assay kit (Bio-Rad Laboratories, Hercules, CA, USA) and protein concentration was measured using the Bio-Rad protein assay kit (Bio-Rad Laboratories), according to the manufacturer's instruction. An equal amount of protein from the samples was separated by denaturing sodium dodecyl sulfate (SDS)-polyacrylamide gel electrophoresis, and then transferred onto polyvinylidene difluoride membranes (Schleicher & Schuell, Keene, NH, USA). The membranes were blocked with 5% skim milk in Tris-buffered saline containing 0.1% Triton X-100 (TBST) for 1 h, and then probed with specific primary antibodies (Santa Cruz Biotechnology, Santa Cruz, CA, USA) to react with the blotted membranes at 4°C overnight. After washing with TBST, the membranes were incubated with the appropriate horseradish peroxidase (HRP)-conjugated secondary antibodies (Santa Cruz Biotechnology, Inc.) for 2 h at room temperature. The expression of protein was detected by enhanced chemiluminescence (ECL) kit (GE Healthcare Life Sciences, Little Chalfont, UK), and visualized by Fusion FX Image system (Vilber Lourmat, Torcy, France).

2.10. Wound healing assay

B16F10 cells were seeded in a 6-well plate (1×10^6 cells/well) and incubated to 80-90% confluence. To evaluate cell migration, wound lines in the form of a cross were made by scraping with a plastic 200 μL pipette tip in confluent cells. After wounding, floating cells were washed out with PBS, and were incubated with 1% FBS-containing DMEM supplemented with or without EEAD for 24 h. Subsequently, the width of wound healing was observed and photographed under a phase-contrast microscope.

2.11. Invasion assay

The invasion ability was assessed using the Trans-well chamber system (10 mm diameter, 8 μm pore size with polycarbonate membrane, Corning Costar Corp., Cambridge, MA, USA). After maintaining B16F10 cells in serum-free DMEM for 24 h, the cells (5×10^4 cells/well) were placed in the upper chamber of trans-well insert, and at the same time, 10% FBS-containing complement medium supplemented with or without EEAD was added into the lower chamber, and then cells were incubated for 24 h. Cells that invaded through the filter were fixed with 3.7% paraformaldehyde, and stained with hematoxylin and eosin (Sigma-Aldrich Chemical Co.). The stained colonies were observed and counted under a phase-contrast microscope and photographed.

2.12. Colony formation assay

After treatment with EEAD for 24 h, single-cell suspensions of B16F10 cells were inoculated on 6-well plates (200 cells/well). The cells were cultured for two weeks while replacing the medium every 3 days to form colonies. The colonies were fixed with 3.7% paraformaldehyde and then stained with 0.1% crystal violet solution (Sigma-Aldrich Chemical Co.) at room temperature for 10 min. The stained colonies were observed and counted under a phase-contrast microscope and photographed.

2.13. Matrix metalloproteinase (MMP) activity assay

The cells were treated with EEAD for 24 h, and then cell culture supernatants were collected to measure the activities of MMP-2 and -9. The activities of MMP-2 and -9 were determined using Biotrak Activity Assay system from Amersham Biosciences (Piscataway, NJ, USA), according to the manufacturer's instruction.

2.14. Animal and *in vivo* experimental procedures

C57BL/6 mice (male, 8 weeks old) were obtained from Samtaco Korea (Osan, Korea). The animals were housed under specific pathogen-free conditions at a temperature of 24 ± 1˚C and humidity of 55 ± 5% in a laminar air-flow room with a 12 h light and 12 h dark circle. After

acclimatization for 1 week, 28 mice were injected intravenously *via* tail vein with 3×10^5 B16F10 cells per 100 μL PBS to produce experimental lung metastasis. At the same time, 16 mice were injected in the same area with PBS alone. After 1 day of tumor inoculation, B16F10 cell injected-mice were randomly divided into three groups: the B16 + control group (100 μL of distilled water), the B16 + EEAD 100 group (100 μL of EEAD 100 mg/kg/day), and the B16 + EEAD 200 group (100 μL of EEAD 200 mg/kg/day). Eighteen PBS-injected mice were also randomly divided into two groups: the normal group (100 μ of distilled water); and the EEAD 200 group (200 μL of EEAD 200 mg/kg/day). All treatments were administrated orally once per day in the morning for 21 days. Mice were sacrificed at day 21 after B16F10 melanoma cells injection, and blood was placed in heparinized tubes, centrifuged at 3,000 rpm for 10 min at 4°C, and kept at -80°C for subsequent analysis. After perfusion, organs were immediately surgically excised, including liver, kidney, spleen, lung, and thymus, then weighed, and stored at -80°C. Animal experiments were conducted in accordance with the Guidelines for Animal Experimentation of Dong-eui University (Busan, Republic of Korea), approved by the Institutional Animal Care and Research Advisory Committee of Dong-eui University (Reference no. R2017-004).

2.15. Blood biochemical analysis

After 21 days of the experiment, blood samples were collected from the animals in all groups. Alanine aminotransferase (ALT) and aspartate aminotransferase (AST) levels were measured using commercial colorimetric assay kits (Abcam Inc. (Cambridge, UK). Lactate dehydrogenase (LDH) activity and blood urea nitrogen (BUN) level were analyzed using detection kits according to the manufacturer's instructions, which kits were obtained from BioVision Inc. (Milpitas, CA, USA) and antibodies-online GmbH (Aachen, Germany), respectively.

2.16. Immunohistochemical staining for tumor necrosis factor (TNF)-α

Histological analysis for TNF-α immunohistochemistry analysis of the lung tissue was performed as described previously (*25*). In brief, the sections of 5 μm thickness were deparaffinized, rehydrated, cooked in antigen retrieval solution (Abcam, Inc.), and dipped in 3% hydrogen peroxide solution for 30 min. TNF-α antibody (Abcam, Inc.) was then applied, and incubated for 1 h at room temperature. After washing, the sections were incubated with peroxidase conjugated secondary antibody (HRP-labelled goat anti-rabbit IgG antibody, DAKO Corp, Glostrup, Denmark) for 40 min. After washing with PBS, images of the sections were photographed with a microscope (Carl Zeiss).

2.17. Statistical analysis

The results of quantitative studies are reported as mean ± standard deviation (SD) using GraphPad Prism software (version 5.03; GraphPad Software, Inc., La Jolla, CA, USA). All experiments were repeated at least three times. To compare data, One-way analysis of variance (ANOVA) with Dunnett's *post-hoc* test was used, and $p < 0.05$ was considered to indicate a statistically significant difference.

3. Results

3.1. EEAD inhibited cell viability and induced apoptosis in B16F10 cells

In evaluate the cytotoxicity of EEAD on B16F10 cells, cells were treated with different concentrations of EEAD for 24 h, and cell viability was assessed by MTT assay. Figure 1A shows that EEAD significantly reduced B16F10 cells viability in a concentration-dependent manner. Phase-contrast microscopic examination demonstrated that the phenotypic characteristics of EEAD-treated cells exhibited irregular cell outlines, decrease of cell density, shrinkage, and increase of detached cells (Figure 1B, upper panel). Therefore, DAPI staining was performed to determine whether EEAD-induced growth inhibition was associated with apoptosis induction, and it was found that nuclear fragmentation and chromatin condensation formation were increased in EEAD treated cells (Figure 1B, lower panel). The results of flow cytometric analysis also showed that the percentage of apoptotic cells was significantly increased in EEAD-treated cells in a concentration-dependent manner (Figure 1C and D).

3.2. EEAD increased mitochondrial dysfunction and ROS generation in B16F10 cells

We assessed whether mitochondrial dysfunction was involved in the induction of EEAD-induced apoptosis and found that the MMP ($\Delta\Psi m$)-dependent formation of JC-1 aggregates in mitochondria was maintained at a relatively high rate in cells not treated with EEAD. However, JC-1 aggregates were markedly reduced after treatment with EEAD in a concentration-dependent manner (Figure 2A and B), indicating a significant depletion of MMP ($\Delta\Psi m$) after EEAD treatment. DCF-DA staining was applied to investigate whether EEAD-induced mitochondrial dysfunction was associated with increased production of ROS. As depicted in Figures 2C and D, ROS production significantly increased according to the rise in concentration of EEAD. The effects of EEAD on the expression of Bcl-2 family members, which play a critical role in the mitochondria-mediated intrinsic apoptotic pathway, were also determined. As indicated in Figure 2E and

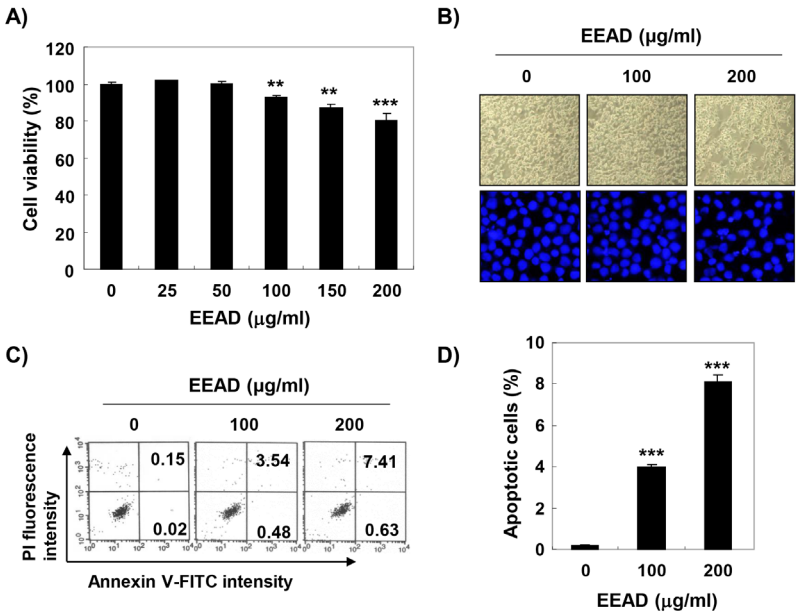

Figure 1. Inhibition of cell viability and induction of apoptosis by EEAD in B16F10 cells. Cells were treated with the indicated concentrations of EEAD for 24 h. **(A)**, The cell viability was assessed by MTT assay. Data are expressed as the mean ± SD. The statistical analyses were conducted using analysis of variance between groups (**$p < 0.001$ and ***$p < 0.0001$ when compared to control). **(B, Upper panel)** Morphological changes of B16F10 cells treated with EEAD for 24 h were observed by a phase-contrast microscope at 40× magnification. **(B, Lower panel)** The nuclear morphological change was observed using DAPI staining, and was photographed under a fluorescence microscope at 400× magnification. Representative photographs of the morphological changes are presented. **(C** and **D)** Apoptosis of B16F10 cells treated with EEAD was measured by flow cytometric analysis using annexin V-FITC and PI. **(C)** Representative profiles. The results show early apoptosis, defined as annexin V^+ and PI^- cells (lower right quadrant), and late apoptosis, defined as annexin V^+ and PI^+ (upper right quadrant) cells. **(D)** The percentages of apoptotic cells were determined by expressing the numbers of Annexin V^+ cells as percentages of all the present cells. The statistical analyses were conducted using analysis of variance between groups (***$p < 0.0001$ when compared to control).

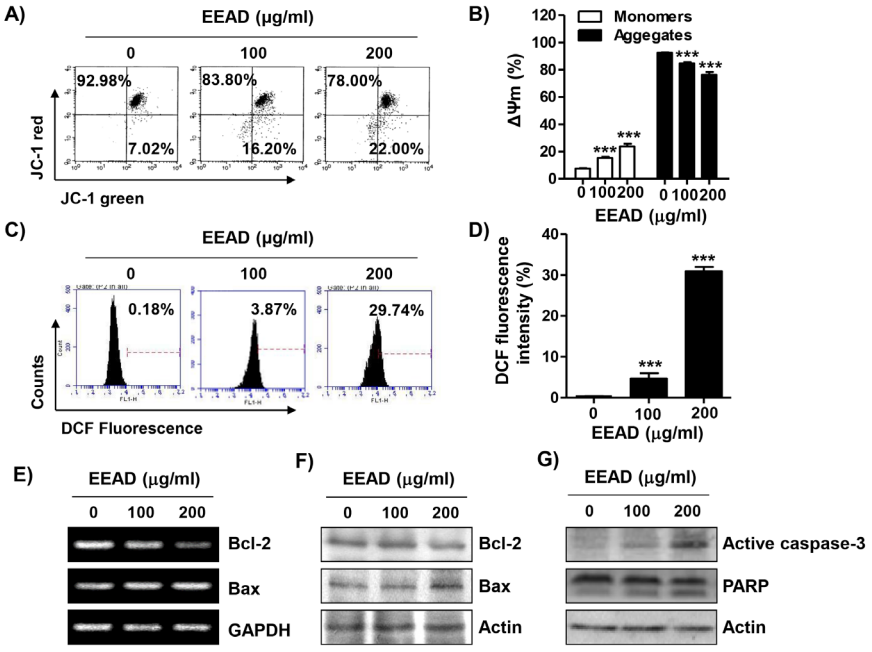

Figure 2. Reduction of MMP (*ΔΨm*) and induction of ROS generation by EEAD in B16F10 cells. (A), After 24 h incubation with the indicated concentrations of EEAD, the cells were stained with JC-1 dye, and were then analyzed by flow cytometry, in order to evaluate the changes in MMP (*ΔΨm*). **(B)** Each bar represents the percentage of cells with JC-1 aggregates and monomers. The quantitative data are expressed in the bar diagram as the mean ± SD. The statistical analyses were conducted using analysis of variance between groups (***$p < 0.0001$ when compared to control). **(C)** The cells were treated with the indicated concentrations of EEAD for 30 min and then intracellular ROS generation was measured by flow cytometry using DCF-DA dye. **(D)** Each bar represents the mean ± SD of three independent experiments (***$p < 0.0001$, when compared to control). **(E)** After treatment with EEAD for 24 h, total RNA was isolated and RT-PCR was performed using the indicated primers. The amplified PCR products were run on 1% agarose gels and visualized with EtBr staining. GAPDH was used as the housekeeping control gene. **(F** and **G)** The cells were lysed and equal amounts of cell lysates were separated by SDS-polyacrylamide gel electrophoresis and transferred to membranes. The membranes were probed with the indicated antibodies and the proteins were visualized using an ECL detection system. The equivalent loading of proteins in each well was confirmed by actin.

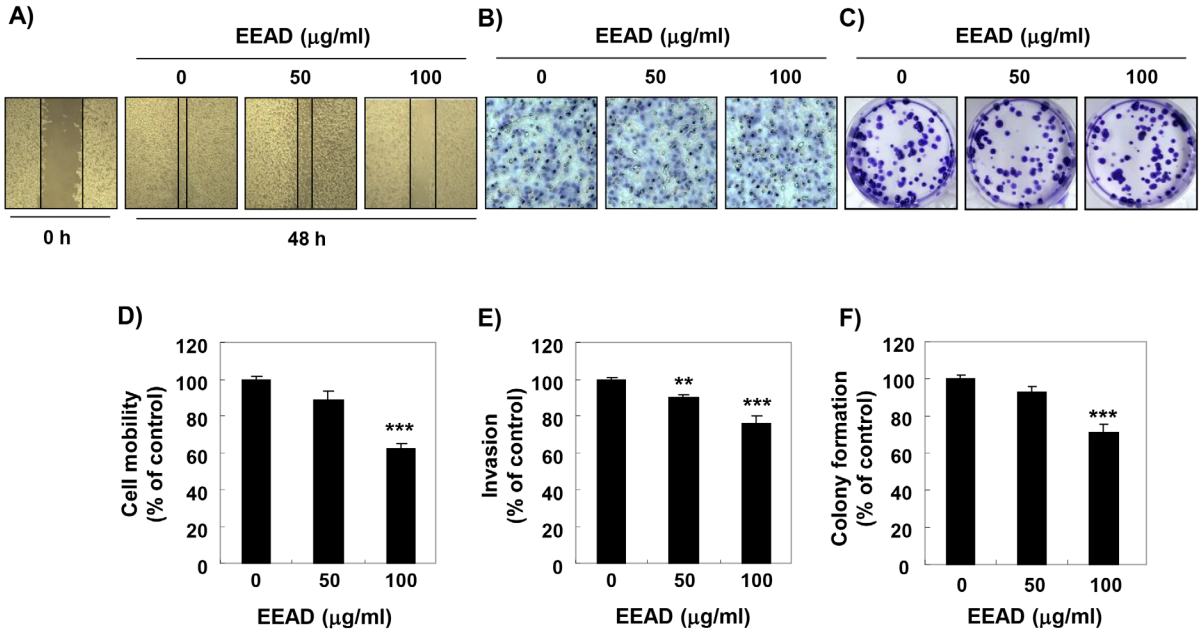

Figure 3. Suppression of cell migration, invasion and colony formation by EEAD in B16F10 cells. (A) Cell migration of B16F10 cells was assessed by wound healing assay at 24 h after EEAD treatment. **(B)** For cell invasion assay using trans-well chamber system, B16F10 cells were placed in the upper chamber of trans-well insert, and complement medium supplemented with EEAD was added in the lower chamber, and then cells were incubated for 24 h. **(C)** B16F10 cells were exposed to EEAD for 15 days, followed by colony formation assay. Cells were stained with 0.1% crystal violet solution, and visualized colonies were observed under a phase-contrast microscope. (A-C) Representative photographs are shown from three independent experiments. **(D)** The mobility of B16F10 cells was calculated for EEAD-treated cells, as compared with the non-treated control cells for each experiment in different field. **(E)** The numbers of invading cells in EEAD-treated cells, as compared with the non-treated control cells, for each experiment. **(F)** Rates of colony formation were detected by microplate reader at 650 nm. The quantitative data are expressed in the bar diagram as the mean ± SD. The statistical analyses were conducted using analysis of variance between groups (**$p < 0.001$ and ***$p < 0.0001$ when compared to control).

F, the levels of pro-apoptotic Bax mRNA and protein were increased, while those of anti-apoptotic Bcl-2 were reduced in EEAD-stimulated cells. EEAD further activated caspase-3 and induced cleavage of poly (ADP-ribose) polymerase (PARP), one of the major substrate proteins of activated caspase-3 (Figure 3G).

3.3. EEAD supprerssed the motility, invasion and colony formation of B16F10 cells *via* the inhibition of MMPs expression and activity

To determine the effect of EEAD on metastatic activity of B16F10 cells, we investigated the cell migration and invasion using wound scratch assay and trans-well system, respectively. Figure 3A and D show that EEAD suppressed the closure rate of the scratch at 24 h treatment, compared with the control cells. Additionally, EEAD apparently decreased the intrusion of B16F10 cells concentration-dependently in trans-well chamber assay (Figure 3B and E), consistent with the result of the wound scratch assay. We also found that the colony forming ability of B16F10 cells was markedly decreased by EEAD relative to the control (Figure 3C and F). Because the degradation of extracellular matrix (ECM) is an essential step in cancer cell metastasis, we investigated whether EEAD regulates the activity and expression of matrix MMPs. Our RT-PCR and immunoblotting results indicated that EEAD effectively decreased the mRNA and protein expression of MMP-2 and -9 (Figure 4A and B), which was associated with a decrease in their enzymatic activity (Figure 4C). However, EEAD concentration-dependently increased the mRNA and protein expression of tissue inhibitor matrix metalloproteinase (TIMP)-1 and -2 (Figure 4A and B).

3.4. EEAD administration reduced the lung metastasis of B16F10 cells in C57BL/6 mice

To examine the effect of EEAD on lung metastasis *in vivo*, we used the lung metastatic mouse model, by which B16F10 melanoma cells were injected into the tail vein of C57BL/6 mice. A total of 44 mice were involved in the present experiment. Twenty-eight mice were injected with B16F10 cells, and 16 mice were injected with PBS as vehicle. From one day after, EEAD 100 mg/kg, EEAD 200 mg/kg, or distilled water were administrated orally once per day in the morning for 21 days. One day after tumor cell inoculation, one animal died in the control group, and one in the EEAD 200 mg/kg group. In the control group, two of them died 14 days after tumor inoculation, and the survival rate on the 21 days was 83.33%. However, the survival rate was not significantly different between

the control and EEAD groups. At day 21, 100% of the normal mice and the EEAD 200 mg/kg treated mice without B16F10 cell inoculation were still alive. During the experimental period, the initial and final body weight did not differ between all the groups (Data not shown). Mice were sacrificed at day 21 of treatment, and their organs were surgically excised. As shown in Table 1, the weight of thymus, spleen, liver and kidney were not significantly different between all groups, exclusive of lung. The B16F10 cells-injected control mice markedly increased lung hypertrophy (2.87-fold of lung weight in normal), whereas it was substantially decreased by EEAD 200 mg/kg treatment. In addition, the levels of BUN showed no significant differences for all groups (Table 2). In contrast, the activities of plasma ALT and AST were elevated in 34.20 and 324.11 U/L, respectively, in B16F10 cells-injected control mice, compared to 23.75 and 126.55 U/L in the normal group, whereas the activities of these enzymes were decreased, following the administration of EEAD. Meanwhile, the LDH activity was apparently increased to 1,042.85 U/L in B16F10 cells-injected control mice (757.60 U/L). However, the LDH activity was meaningfully decreased by the administration of EEAD 200 mg/kg, and its activity was similar to that of the normal mice. Next, we investigated the effect of EEAD on the histopathological alteration of lung metastatic tissue following B16F10 inoculation. The number of metastatic tumor nodules in B16F10-injected control mice was apparently increased in comparison with normal mice visually (Figure 5A), as well as numerically (Figure 5B). In contrast, the number of metastatic tumor nodules was significantly reduced by the oral administration of EEAD, in a concentration-dependent manner. In addition, we evaluated whether EEAD could suppress lung inflammation in these mice. Similar to the results from the count of metastatic tumor, Figure 5C shows that TNF-α of lung metastatic tissue was overexpressed in B16F10 cell inoculated-mice, but completely inhibited in EEAD-treated mice.

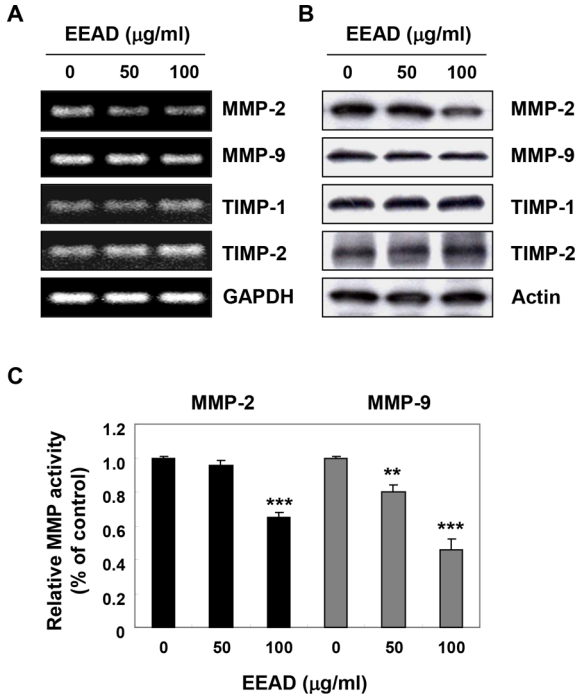

Figure 4. Inhibition of the expression and activity of MMP-2 and -9 by EEAD in B16F10 cells. (A) After treatment with EEAD for 24 h, total RNA was isolated and RT-PCR was performed using the indicated primers. The amplified PCR products were run on 1% agarose gels and visualized with EtBr staining. GAPDH was used as the housekeeping control gene. **(B)** The cells were lysed and equal amounts of cell lysates were separated by SDS-polyacrylamide gel electrophoresis and transferred to membranes. The membranes were probed with the indicated antibodies and the proteins were visualized using an ECL detection system. The equivalent loading of proteins in each well was confirmed by actin. **(C)** *In vitro* activity of MMP-2 and -9 in cell culture supernatant was measured using a MMP-2 and -9 gelatinase activity assay kit. Data are mean ± SD deviation from three independent experiments and are presented as fold change compared with vector control (**$p < 0.001$ and ***$p < 0.0001$ when compared to control).

4. Discussion

Apoptosis, a well known programmed cell death, is an essential mechanism to maintain cell homeostasis and maintains a balance between cell survival and apoptosis (*26,27*). Cancer develops as a result of a

Table 1. The effects of oral administration of EEAD on organ weights in B16F10 cells-inoculated C57BL/6 mice

Group	No. of animals	Organ weights (g)				
		Thymus	Lung	Spleen	Liver	Kidney
Normal	8	0.050 ± 0.094	0.15 ± 0.01	0.075 ± 0.008	1.38 ± 0.06	0.37 ± 0.06
EEAD 200	8	0.049 ± 0.011	0.15 ± 0.02	0.075 ± 0.009	1.32 ± 0.03	0.37 ± 0.01
B16 + control	8	0.045 ± 0.009	0.43 ± 0.15	0.086 ± 0.017	1.39 ± 0.10	0.37 ± 0.03
B16 + EEAD 100	8	0.043 ± 0.007	0.35 ± 0.25	0.086 ± 0.019	1.34 ± 0.09	0.36 ± 0.04
B16 + EEAD 200	8	0.044 ± 0.009	0.20 ± 0.17	0.080 ± 0.024	1.37 ± 0.05	0.37 ± 0.02

After 1 day of tumor inoculation, B16F10 cell injected-mice were randomly divided into three groups: the B16+control group (100 μl of distilled water), the B16+EEAD 100 group 100 μL of EEAD 100 mg/kg/day), and the B16+EEAD 200 group (100 μL of EEAD 200 mg/kg/day). PBS-injected mice were also randomly divided into two groups: the normal group (100 μ of distilled water); and the EEAD 200 group (200 μL of EEAD 200 mg/kg/day). Mice were sacrificed at day 21 after B16F10 melanoma cells injection, and thymus, lung, spleen, liver, and kidney were immediately surgically excised, and then measured the weight. Data are presented as means ± SD.

Table 2. The effects of oral administration of EEAD to AST, ALT, BUN, and LDH values of serum samples obtained from B16F10 cells-inoculated C57BL/6 mice

Group	No. of animals	ALT (U/L)	AST (U/L)	BUN (mg/dL)	LDH (U/L)
Normal	8	23.75 ± 3.10	126.55 ± 55.86	20.11 ± 2.38	757.60 ± 87.08
EEAD 200	8	22.94 ± 2.47	123.09 ± 31.17	20.19 ± 3.14	699.47 ± 89.41
B16 + control	8	34.20 ± 6.63	324.11 ± 90.03	20.66 ± 7.24	1042.85 ± 57.03
B16 + EEAD 100	8	31.11 ± 9.59	299.11 ± 87.17	20.79 ± 2.47	1001.00 ± 12.47
B16 + EEAD 200	8	28.97 ± 7.14	227.67 ± 97.17	19.98 ± 2.77	874.95 ± 93.14

After 1 day of tumor inoculation, B16F10 cell injected-mice were randomly divided into three groups: the B16 + control group (100 μl of distilled water), the B16 + EEAD 100 group (100 μl of EEAD 100 mg/kg/day), and the B16 + EEAD 200 group (100 μL of EEAD 200 mg/kg/day). PBS-injected mice were also randomly divided into two groups: the normal group (100 μ of distilled water); and the EEAD 200 group (200 μL of EEAD 200 mg/kg/day). The whole blood of mice was collected after 21 day treatment with or without EEAD. The values of ALT, AST, BUN, and LDH were measured. Data are presented as means ± SD.

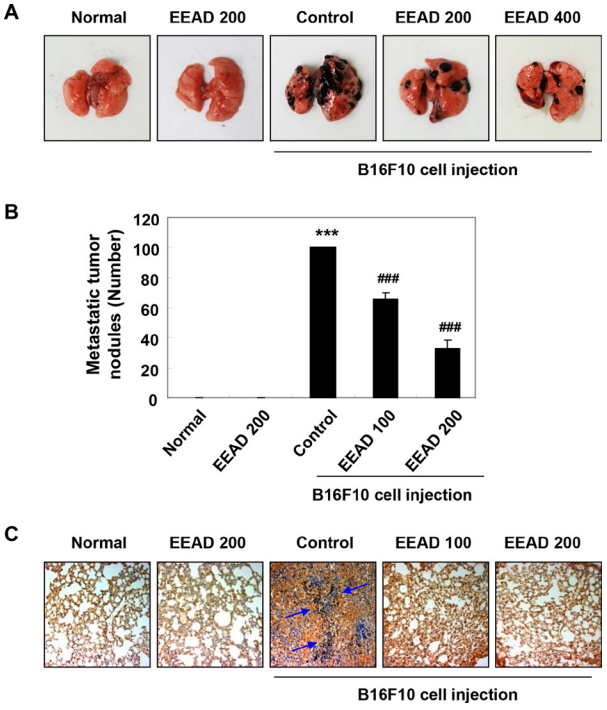

Figure 5. Effects of EEAD on pulmonary metastasis of B16F10 melanoma cells *in vivo*. (A) Representatives of metastatic nodules on the surface of the lungs in C57BL/6 mice induced by injecting 3×10^5 cells intravenously, which were then treated daily with 100 and 150 mg/kg EEAD. On day 21, the mice were sacrificed, and their lungs were then removed and fixed. Metastatic foci at the lung surfaces were photographed. **(B)** The number of metastatic nodules in each group were counted, and data presented as the mean ± SD (n = 8). The statistical analyses were conducted using analysis of variance between groups (***$p < 0.0001$ when compared to normal group. ###$p < 0.0001$ when compared to B16F10 cell-injected control group). **(C)** Tumor tissues of lung metastasis were immunohistochemistry stained with TNF-α. Blue arrow indicates the TNF-α-expressed area shown in brown color, and marks the metastasis nodule (Original magnification, 200×).

series of genetic changes, during which normal cells are converted to malignant cells that are involved in abnormal growth and uncontrolled growth of cells (*28,29*). Hence, most chemotherapeutic agents function by inducing apoptosis in malignant cells, so the induction of apoptosis is a major strategy for cancer treatment and one of the most actively studied areas (*30,31*). In the present study, we have verified that EEAD, ethanol extract from the *Angelica dahurica Radix*, suppressed B16F10 cell proliferation in a concentration-dependent manner. Additionally, EEAD significantly increased the percentage of annexin V^+-positive cells. Furthermore, EEAD-treated cells showed the typical morphological hallmarks of apoptotic cells, such as chromatin condensation, nuclear fragmentation, and cell shrinkage. These results suggest that the inhibition of cell growth by EEAD is associated with the induction of apoptosis in B16F10 melanoma cells.

Apoptosis is largely divided into death receptor (DR)-mediated extrinsic and mitochondria-mediated intrinsic pathways (*26,28*). The extrinsic pathway begins with the activation of caspase-8 by the formation of the death-inducing signaling complex through the binding of death ligand to the cell surface DR (*27,32*). On the other hand, the intrinsic apoptosis signal pathway is initiated by genetic damage, oxidative stress, hypoxia, and high concentration of cytosolic Ca^{2+}, which converge at the mitochondria (*28,33*). This pathway is the result of a mitochondrial dysfunction that includes loss of MMP ($\Delta\psi m$), production of ROS, opening of the permeability transition pore, and release of cytochrome *c* from the mitochondria to the cytoplasm, which is strictly regulated by a group of proteins that are composed of pro- and anti-apoptotic proteins, such as Bcl-2 protein family proteins (*33,34*). The release of cytochrome *c* eventually activates caspase-3 *via* the formation of apoptosome, which consists of cytochrome *c*, caspase-9, and Apaf-1 (*28,34*). Caspase-3 converges both intrinsic and extrinsic pathways, and degrades various substrate proteins, such as PARP (*27,34*). In the current study, we investigated whether apoptosis by EEAD was associated with mitochondria dysfunction. Our results showed that EEAD significantly increased MMP ($\Delta\psi m$) loss, as well as intracellular accumulation of ROS, in B16F10 melanoma cells. Moreover, EEAD increased the expression of pro-apoptotic Bax and inhibited the expression of anti-apoptotic Bcl-2. Additionally, EEAD induced the activation of caspase-3, and the degradation of PARP. Therefore, these results demonstrate that

EEAD induced apoptosis through a mitochondria-mediated intrinsic pathway in B16F10 melanoma cells.

Melanoma, one of the most aggressive malignancies, is a skin cancer with a resistance to cytotoxic anti-tumor drugs, and high capacity for invasion and metastasis (*1,2*). Therefore, the rate of response of standard therapies is low and prognosis is also poor. This is estimated to be because melanocytes originate from highly motile cells that have enhanced survival properties (35,36). Metastasis is caused by the movement of cancer cells from the primary tumor to target organs, thus blocking cancer cell migration and invasion, which are most important for the treatment of melanoma (*37,38*). Herein, we found that EEAD suppressed the migration and invasion of B16F10 cells through the results of wound scratch assay and trans-well assay, in the concentration range of non-toxic conditions. In addition, we confirmed that EEAD also inhibited anchorage-dependent colony formation that is a characteristic of tumor cells (*39,40*). These results indicate that EEAD blocked the migration and invasion, key steps of the metastasis of cancer cell, as well as the establishment of anchorage-dependent colony formation from a single cell. Degradation and remodeling of the ECM and basement membranes are essential steps in the metastasis of melanoma. These processes are mediated by proteolytic enzymes, such as MMPs and their tissue inhibitors, TIMPs, and the regulation of their expression and/or activation on invasion and migration in many types of tumors has been widely reviewed *in vitro* and *in vivo* (*41,42*). In particular, MMP-2 and -9 are well known to induce cancer progression and the metastasis of melanoma through the degradation of type IV collagen, which is the major component of the basement membrane (*43,44*). In this regard, we demonstrated that EEAD markedly decreased the activity of MMP-2 and -9. Furthermore, our results proved that EEAD induced the down-regulated expression of MMP-2 and -9, as well as the up-regulated expression of TIMP-1 and -2 in mRNA and protein levels. Based on these findings, we suggest that EEAD promotes an increase of TIMP/MMPs ratio as a critical factor in the regulation of the motility of melanoma cells, which may subsequently lead to the suppression of cell migration and invasion associated metastasis.

Furthermore, we have re-confirmed the efficacy of EEAD on the suppression of metastasis in B16F10 cell inoculated-mice. Interestingly, B16F10 cells have been metastasized specifically to the lung following the injection into the tail vein, and most of the cells have been found in the pulmonary tissue (*45*). Therefore, the murine B16F10 melanoma is most accepted as a useful model for metastatic lung tumor, its application having been used to evaluate the metastatic mechanisms of melanoma and the development of anti-cancer therapies (*45,46*). Numerous studies reported the experimental pulmonary metastasis model by B16F10 cell inoculation in C57BL/6 mice, and investigated the efficacy of new potential anti-cancer agents in this murine model (*47-49*). In the current study, we identified that B16F10 cell inoculated-mice have induced lung hypertrophy and increase of the number and expression of metastatic tumor nodules in lung tissue, whereas these were significantly decreased by the oral administration of EEAD. Additionally, the oral administration of EEAD reduced serum LDH activity, as the most consistent marker of the aggressive carcinogenesis (*50*), without weight loss or nephrotoxicity. Similarly, plasma levels of ALT and AST, which are considered to be important indicators for measuring liver damage (*51,52*), in B16F10 cell-inoculated mice were higher than those of the normal group. However, they were dose-dependently reduced by oral administration of EEAD. These results suggest that EEAD can be a considerably safe therapeutic candidate for metastatic melanoma through its low toxicity, and efficacy in the suppression of metastasis. Moreover, our study also provided that B16F10 inoculation enhanced the expression of TNF-α in the metastatic region, but was suppressed by EEAD. It is well known that inflammation plays principal roles at different stages of tumor development, including initiation, promotion, malignant conversion, invasion, and metastasis (*53,54*). El Rayes *et al*. (*55*) demonstrated that lung inflammation promotes metastasis, and Yu et al. (*56*) reported pro-inflammatory cytokines, including TNF-α, interleukin (IL)-1 and IL-6, accelerate MMPs expression, invasiveness, and metastasis. In this respect, our results provide the possibility of EEAD suppressing inflammation, a hallmark of cancer contributing to tumor development, and may lead to the inhibition of metastasis in lung cancer.

As has been mentioned, melanoma is a tumor with a resistance to drugs therapies (*1,2*). To solve this problem, a lot of researches are getting identification of the mechanisms by which melanoma initiation can be triggered and sustained. Recently, there are well known that melanoma may trigger not only the activation of RAS/MEK singling pathway, but also other pathways such as phosphoinositide 3-kinase (PI3K)/Akt and Wnt signaling pathways (*57,58*). In present study, we found that exposure to EEAD led to decrease protein expression of Akt and β-catenin in B16F10 cells (Supplementary Figure S1, *http://www.biosciencetrends.com/action/getSupplementalData.php?ID=55*). These results suggested that EEAD suppressed tumor growth *via* down-regulation of Akt and β-catenin pathway, but not RAS/MEK pathway. Although we have partially identified the underlying mechanism of EEAD on suppression of melanoma tumor, action mechanism and efficacy of bioactive components from *Angelica dahurica Radix* needs to be confirmed. Recent discoveries reported that coumarin

and pyrrole 2-carbaldedhyde derived alkaloids from *Angelica dahurica Radix* were identified and have bioactivity (*59,60*). In this context, further studies are need to investigate whether these active compounds also have anti-cancer effects for melanoma, as well as identify the underlying actin mechanism.

In summary, EEAD inhibited B16F10 melanoma cell growth through the induction of mitochondria-mediated intrinsic apoptosis pathway. EEAD also promoted down-regulation of MMPs activity and expression, which is a critical factor in the regulation of the motility of melanoma cells, and may subsequently lead to the suppression of cell migration and invasion-associated metastasis. In the metastatic lung cancer mouse, EEAD inhibited lung hypertrophy and metastatic tumor nodule, as well as inflammation in lung tissue without toxicity. Although the identification of bioactive components of EEAD should be performed, the results of this study suggest that EEAD may be a potential anti-invasive candidate for treatment strategies for metastatic melanoma tumors.

Acknowledgements

This research was funded by Basic Science Research Program through the National Research Foundation of Korea (NRF) grant funded by the Korea government (2018R1A2B2005705).

References

1. Read T, Lonne M, Sparks DS, David M, Wagels M, Schaider H, Soyer HP, Smithers BM. A systematic review and meta-analysis of locoregional treatments for in-transit melanoma. J Surg Oncol. 2019; 119: 887-896.
2. Weitman ES, Zager JS. Regional therapies for locoregionally advanced and unresectable melanoma. Clin Exp Metastasis. 2018; 35:495-502.
3. Almeida FV, Douglass SM, Fane ME, Weeraratna AT. Bad company: Microenvironmentally mediated resistance to targeted therapy in melanoma. Pigment Cell Melanoma Res. 2019; 32:237-247.
4. Swe T, Kim KB. Update on systemic therapy for advanced cutaneous melanoma and recent development of novel drugs. Clin Exp Metastasis. 2018; 35:503-520.
5. Herrington CS, Poulsom R, Coates PJ. Recent advances in pathology: the 2019 annual review issue of the journal of pathology. J Pathol. 2019; 247:535-538.
6. Amaral T, Meraz-Torres F, Garbe C. Immunotherapy in managing metastatic melanoma: which treatment when? Expert Opin Biol Ther. 2017; 17:1523-1538.
7. Danciu C, Soica C, Antal D, Alexa E, Pavel IZ, Ghiulai R, Ardelean F, Babuta RM, Popescu A, Dehelean CA. Natural compounds in the chemoprevention of malignant melanoma. Anticancer Agents Med Chem. 2018; 18:631-644.
8. Albuquerque KRS, Pacheco NM, Del Rosario Loyo Casao T, de Melo FCSA, Novaes RD, Gonçalves RV. Applicability of plant extracts in preclinical studies of melanoma: A systematic review. Mediators Inflamm. 2018; 2018:6797924.
9. Prieto JM, Silveira D. Natural cytotoxic diterpenoids, a potential source of drug leads for melanoma therapy. Curr Pharm Des. 2018; 24:4237-4250.
10. Wei H, Xiao Y, Tong Y, Chen Y, Luo X, Wang Y, Jin P, Ma C, Fu Z, Guo H, Zhao X, Li Y. Therapeutic effect of angelica and its compound formulas for hypertension and the complications: Evidence mapping. Phytomedicine. 2019; 59:152767.
11. Sowndhararajan K, Deepa P, Kim M, Park SJ, Kim S. A review of the composition of the essential oils and biological activities of *Angelica* species. Sci Pharm. 2017; 85:E33.
12. Sarker SD, Nahar L. Natural medicine: the genus Angelica. Curr Med Chem. 2004; 11:1479-1500.
13. Li D, Wu L. Coumarins from the roots of *Angelica dahurica* cause anti-allergic inflammation. Exp Ther Med. 2017; 14:874-880.
14. Wang GH, Chen CY, Tsai TH, Chen CK, Cheng CY, Huang YH, Hsieh MC, Chung YC. Evaluation of tyrosinase inhibitory and antioxidant activities of *Angelica dahurica* root extracts for four different probiotic bacteria fermentations. J Biosci Bioeng. 2017; 123:679-684.
15. Lee HJ, Lee H, Kim MH, Choi YY, Ahn KS, Um JY, Lee SG, Yang WM. *Angelica dahurica* ameliorates the inflammation of gingival tissue *via* regulation of pro-inflammatory mediators in experimental model for periodontitis. J Ethnopharmacol. 2017; 205:16-21.
16. Lee MY, Lee JA, Seo CS, Ha H, Lee H, Son JK, Shin HK. Anti-inflammatory activity of *Angelica dahurica* ethanolic extract on RAW264.7 cells *via* upregulation of heme oxygenase-1. Food Chem Toxicol. 2011; 49:1047-1055.
17. Zheng YM, Shen JZ, Wang Y, Lu AX, Ho WS. Anti-oxidant and anti-cancer activities of *Angelica dahurica* extract *via* induction of apoptosis in colon cancer cells. Phytomedicine. 2016; 23:1267-1274.
18. Yang WQ, Song YL, Zhu ZX, Su C, Zhang X, Wang J, Shi SP, Tu PF. Anti-inflammatory dimeric furanocoumarins from the roots of *Angelica dahurica*. Fitoterapia. 2015; 105:187-193.
19. Mi C, Ma J, Wang KS, Zuo HX, Wang Z, Li MY, Piao LX, Xu GH, Li X, Quan ZS, Jin X. Imperatorin suppresses proliferation and angiogenesis of human colon cancer cell by targeting HIF-1α *via* the mTOR/p70S6K/4E-BP1 and MAPK pathways. J Ethnopharmacol. 2017; 203:27-38.
20. Wu M, Li T, Chen L, Peng S, Liao W, Bai R, Zhao X, Yang H, Wu C, Zeng H, Liu Y. Essential oils from *Inula japonica* and *Angelicae dahuricae* enhance sensitivity of MCF-7/ADR breast cancer cells to doxorubicin *via* multiple mechanisms. J Ethnopharmacol. 2016; 180:18-27.
21. Li X, Zeng X, Sun J, Li H, Wu P, Fung KP, Liu F. Imperatorin induces Mcl-1 degradation to cooperatively trigger Bax translocation and Bak activation to suppress drug-resistant human hepatoma. Cancer Lett. 2014; 348:146-155.
22. Choochuay K, Chunhacha P, Pongrakhananon V, Luechapudiporn R, Chanvorachote P. Imperatorin sensitizes anoikis and inhibits anchorage-independent growth of lung cancer cells. J Nat Med. 2013; 67:599-606.
23. Koh EM, Lee EK, Song CH, Song J, Chung HY, Chae CH, Jung KJ. Ferulate, an active component of wheat

germ, ameliorates oxidative stress-induced PTK/PTP imbalance and PP2A inactivation. Toxicol Res. 2018, 34:333-341.
24. Kang JB, Kim DK, Park DJ, Shah MA, Kim MO, Jung EJ, Lee HS, Koh PO. Hyperglycemia aggravates decrease in alpha-synuclein expression in a middle cerebral artery occlusion model. Lab Anim Res. 2018; 34:195-202.
25. Kwon HJ, Jung HY, Hahn KR, Kim W, Kim JW, Yoo DY, Yoon YS, Hwang IK, Kim DW. *Bacopa monnieri* extract improves novel object recognition, cell proliferation, neuroblast differentiation, brain-derived neurotrophic factor, and phosphorylation of cAMP response element-binding protein in the dentate gyrus. Lab Anim Res. 2018; 34:239-247.
26. Pfeffer CM, Singh ATK. Apoptosis: A target for anticancer therapy. Int J Mol Sci. 2018, 19:448.
27. Hassan M, Watari H, AbuAlmaaty A, Ohba Y, Sakuragi N. Apoptosis and molecular targeting therapy in cancer. Biomed Res Int. 2014; 2014:150845.
28. Kiraz Y, Adan A, Kartal Yandim M, Baran Y. Major apoptotic mechanisms and genes involved in apoptosis. Tumour Biol. 2016; 37:8471-8486.
29. Hanahan D, Weinberg RA. Hallmarks of cancer: the next generation. Cell. 2011; 144:646-674.
30. Bolhassani, A. Cancer chemoprevention by natural carotenoids as an efficient strategy. Anticancer Agents Med Chem. 2015; 15:1026-1231.
31. Medema RH, Macůrek L. Checkpoint control and cancer. Oncogene. 2012; 31:2601-2613.
32. Kantari C, Walczak H. Caspase-8 and bid: caught in the act between death receptors and mitochondria. Biochim Biophys Acta. 2011, 1813:558-563.
33. Schultz, DR, Harrington WJ Jr. Apoptosis: programmed cell death at a molecular level. Semin. Arthritis Rheum. 2003, 32:345-369.
34. Edlich F. BCL-2 proteins and apoptosis: Recent insights and unknowns. Biochem Biophys Res Commun. 2018, 500:26-34.
35. Helgadottir H, Rocha Trocoli Drakensjö I, Girnita A. Personalized medicine in malignant melanoma: Towards patient tailored treatment. Front Oncol. 2018; 8:202.
36. Gray-Schopfer V, Wellbrock C, Marais R. Melanoma biology and new targeted therapy. Nature. 2007; 445:851-857.
37. Huang R, Rofstad EK. Integrins as therapeutic targets in the organ-specific metastasis of human malignant melanoma. J Exp Clin Cancer Res. 2018; 37:92.
38. Arena GO, Arena V, Arena M, Abdouh M. Transfer of malignant traits as opposed to migration of cells: A novel concept to explain metastatic disease. Med Hypotheses. 2017; 100:82-86.
39. Achkova D, Maher J. Role of the colony-stimulating factor (CSF)/CSF-1 receptor axis in cancer. Biochem Soc Trans. 2016; 44:333-341.
40. Russo J, Russo IH. The role of the basal stem cell of the human breast in normal development and cancer. Adv Exp Med Biol. 2011; 720:121-134.
41. Gonzalez-Avila G, Sommer B, Mendoza-Posada DA, Ramos C, Garcia-Hernandez AA, Falfan-Valencia R. Matrix metalloproteinases participation in the metastatic process and their diagnostic and therapeutic applications in cancer. Crit Rev Oncol Hematol. 2019; 137:57-83.
42. Deryugina EI, Quigley JP. Tumor angiogenesis: MMP-mediated induction of intravasation- and metastasis-sustaining neovasculature. Matrix Biol. 2015; 44-46:94-112.
43. Jabłońska-Trypuć A, Matejczyk M, Rosochacki S. Matrix metalloproteinases (MMPs), the main extracellular matrix (ECM) enzymes in collagen degradation, as a target for anticancer drugs. J Enzyme Inhib Med Chem. 2016; 31:177-183.
44. Sampieri CL, León-Córdoba K, Remes-Troche JM. Matrix metalloproteinases and their tissue inhibitors in gastric cancer as molecular markers. J Cancer Res Ther. 2013; 9:356-363.
45. Fidler IJ. The relationship of embolic homogeneity, number, size and viability to the incidence of experimental metastasis. Eur J Cancer. 1973; 9:223-227.
46. Giavazzi R, Decio A. Syngeneic murine metastasis models: B16 melanoma. Methods Mol Biol. 2014; 1070:131-140.
47. Pal S, Amin PJ, Sainis KB, Shankar BS. Potential role of TRAIL in metastasis of mutant KRAS expressing lung adenocarcinoma. Cancer Microenviron. 2016; 9: 77-84.
48. Gautam A, Densmore CL, Waldrep JC. Inhibition of experimental lung metastasis by aerosol delivery of PEI-p53 complexes. Mol Ther. 2000; 2:318-323.
49. Siddikuzzaman, Grace VM. Inhibition of metastatic lung cancer in C57BL/6 mice by liposome encapsulated all trans retinoic acid (ATRA). Int Immunopharmacol. 2012; 14:570-579.
50. Chaube B, Malvi P, Singh SV, Mohammad N, Meena AS, Bhat MK. Targeting metabolic flexibility by simultaneously inhibiting respiratory complex I and lactate generation retards melanoma progression. Oncotarget. 2015; 6:37281-37299.
51. Liu Y, Zhao P, Cheng M, Yu L, Cheng Z, Fan L, Chen C. AST to ALT ratio and arterial stiffness in non-fatty liver Japanese population: a secondary analysis based on a cross-sectional study. Lipids Health Dis. 2018; 17:275.
52. Webster GF, Webster TG, Grimes LR. Laboratory tests in patients treated with isotretinoin: occurrence of liver and muscle abnormalities and failure of AST and ALT to predict liver abnormality. Dermatol Online J. 2017; 23:13030.
53. Ham B, Fernandez MC, D'Costa Z, Brodt P. The diverse roles of the TNF axis in cancer progression and metastasis. Trends Cancer Res. 2016; 11:1-27.
54. Nenu I, Tudor D, Filip AG, Baldea I. Current position of TNF-α in melanomagenesis. Tumour Biol. 2015; 36:6589-6602.
55. El Rayes T, Catena R, Lee S, Stawowczyk M, Joshi N, Fischbach C, Powell CA, Dannenberg AJ, Altorki NK, Gao D, Mittal V. Lung inflammation promotes metastasis through neutrophil protease-mediated degradation of Tsp-1. Proc Natl Acad Sci U S A. 2015; 112:16000-16005.
56. Yu H, Kortylewski M, Pardoll D. Crosstalk between cancer and immune cells: role of STAT3 in the tumour microenvironment. Nat Rev Immunol. 2007; 7:41-51.
57. Dantonio PM, Klein MO, Freire MRVB, Araujo CN, Chiacetti AC, Correa RG. Exploring major signaling cascades in melanomagenesis: a rationale route for targetted skin cancer therapy. Biosci Rep. 2018; 38:BSR20180511.
58. Gray-Schopfer V, Wellbrock C, Marais R. Melanoma biology and new targeted therapy. Nature 2007: 445:851-857.
59. Wang J, Peng L, Shi M, Li C, Zhang Y, Kang W.

Spectrum effect relationship and component knock-out in *Angelica Dahurica Radix* by high performance liquid chromatography-Q exactive hybrid quadrupole-qrbitrap mass spectrometer. Molecules. 2017; 22:E1231.
60. Qi B, Yang W, Ding N, Luo Y, Jia F, Liu X, Wang J, Wang X, Tu P, Shi S. Pyrrole 2-carbaldehyde derived alkaloids from the roots of *Angelica dahurica*. J Nat Med. 2019; 73:769-776.

Received August 25, 2019; Revised December 26, 2019; Accepted January 25, 2020.

**Address correspondence to:*
Yung Hyun Choi, Department of Biochemistry, Dongeui University College of Korean Medicine, 52-57, Yangjeong-ro, Busanjin-gu, Busan 47227, Korea.
E-mail: choiyh@deu.ac.kr

Released online in J-STAGE as advance publication February 25, 2020.